Jour. Fac. Sci., Hokkaido Univ., Ser. VII (Geophysics), Vol. 8, No. 2, 155-172, 1987.

Strong-motion Modeling of the 1980 Izu-Hanto-Toho-Oki Earthquake by Inversion Method

Hiroshi Takenaka

Department of Geophysics, Faculty of Science, Hokkaido University, Sapporo 060, Japan

(Received November 29, 1986)

Abstract

Near-field strong-motion records ($\Delta < 60$ km) are modeled to estimate the spatial distribution of seismic moment for the 1980 Izu-Hanto-Toho-Oki earthquake (M_{JMA} 6.7). An inversion method involving a Mellman's error function is used to interpret the strong-motion waveforms in the period range of 3 to 20 sec. The earthquake source is approximated by point dislocations distributed uniformly and densely over the fault plane. The fault plane is discretized into subfaults each having constant seismic moment. The seismic moments of the subfaults are taken as free parameters in the inversion. Inversion is carried out for different combinations of fault strike, rupture velocity and rise time. Only the combination of a strike of N5°W and a rupture velocity of 3.0 km/sec has reasonable solutions. These solutions have little moment on the northern part of the fault plane, and suggest that there was minimal extension of rupture front to the north during the main shock. By comparison of our solutions with the seismicity before and after the mainshock, it is found that the rupture front could not go across the swarm area near the hypocenter during the mainshock.

1. Introduction

In recent years, many investigators have studied the faulting processes of shallow moderate sized earthquakes in detail. The 1979 Imperial Valley earthquake is a good example of such earthquakes. This earthquake produced high quality digital records of strong motion at short distances from the epicenter. The records were analyzed by using modern waveform synthesis and inversion techniques (e.g. Hartzell and Helmberger, 1982; Olson and Apsel, 1982; Hartzell and Heaton, 1983; Archuleta, 1984).

In Japan, no earthquake has been recorded by networks of digital instruments which supply near-field data suitable for waveform modeling. The strong-motion seismograph network of JMA (Japan Meteorological Agency), however, has provided a wealth of analogue near-field records of fair quality.

The 1980 Izu-Hanto-Toho-Oki earthquake (M_{JMA} 6.7) is one of such earthquakes. This earthquake occurred on 29 June, 1980 (JST), off the east coast of the Izu Peninsula. The most characteristic feature of this earthquake was that a very active earthquake swarm continued in the area very close to its hypocenter just before and after its occurrence. Detailed investigations have been made on the swarm activity and aftershock sequence (e.g. Mastu'ura, 1983).

This paper presents an attempt to model strong-motion displacement records obtained by the JMA stations near the epicenter and derive constraints on the source process of this earthquake. An inversion method is applied to the strong-motion data to estimate the spatial distribution of the seismic moment release during the main shock.

2. Data

Figure 1 shows the location of the epicenter of the 1980 Izu-Hanto-Toho-Oki earthquake and the locations of JMA stations used in this study. Table 1 lists pertinent data of the stations concerning the epicenter. The epicenter has been estimated to be located at 34°53.5′N, 139°13.7′E with a hypocentral depth of

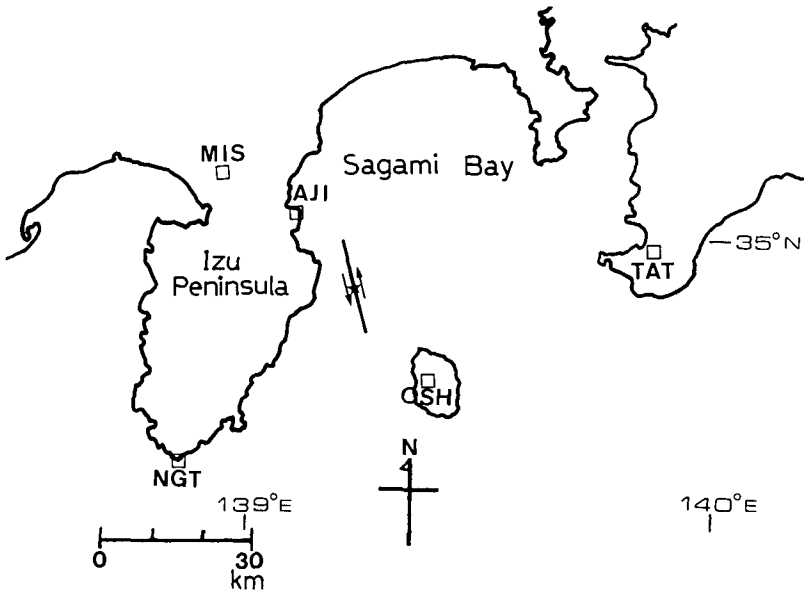

Fig. 1 Location of the epicenter of the 1980 Izu-Hanto-Toho-Oki earthquake and JMA stations whose strong-motion seismograms were analyzed in this study. The star indicates the epicenter. The open squares indicate JMA stations.

Table 1 Station data

Station Code	Epicentral Distance (km)	Azimuth (degrees East of North)
AJI	20.6	324.5
MIS	36.5	311.9
NGT	47.6	227.3
OSH	20.0	136.4
TAT	59.2	80.0

10.5 km (Matsu'ura, 1983). The source mechanism has been estimated to be left-lateral strike-slip in a nearly NS direction (Shimazaki, 1980).

We used the horizontal components of the displacement records obtained by the JMA strong-motion seismographs at Ajiro (AJI), Mishima (MIS), Irozaki (NGT), Tateyama (TAT) and Oshima (OSH) stations (Fig. 2). The EW-component of OSH station could not be used due to significant off-scale (Fig. 2). The instrumental characteristics of the JMA strong-motion seismograph are shown in Table 2. The seismograms were digitized and were corrected for distortions due to zero line shift and finite arm length. After these corrections, the digitized records were linearly interpolated to a uniform time step of 0.25 sec.

Some investigations of the reliability of records obtained by the JMA strong-motion seismographs have been made. Yamada et al. (1985) and Yamanaka et al. (1985) compared many digitized records of the JMA strong-motion seismographs with the records obtained by other broad-band strong-motion seismographs, and found that the former can be reliable in the period range from 2 to 20 sec. Taking into account the results of these investigations, we filtered the digitized records by a Chebyshev band-pass filter (Saito, 1978) with a pass-band of 3 to 20 sec. To guarantee zero phase shift, the filter was applied twice, once in the forword direction and once in the backward direction. Figure 2 shows the raw records and the processed traces.

3. Method

3.1. Finite-fault modeling

The earthquake source is approximated by point dislocations uniformly distributed (1 km spacing) on the fault plane. The fault plane is divided into subfaults on which the seismic moment (equivalent to the weight of individual point source) is supposed to be constant. To reduce the number of inversion parameters as small as possible, we assume that a circular rupture front

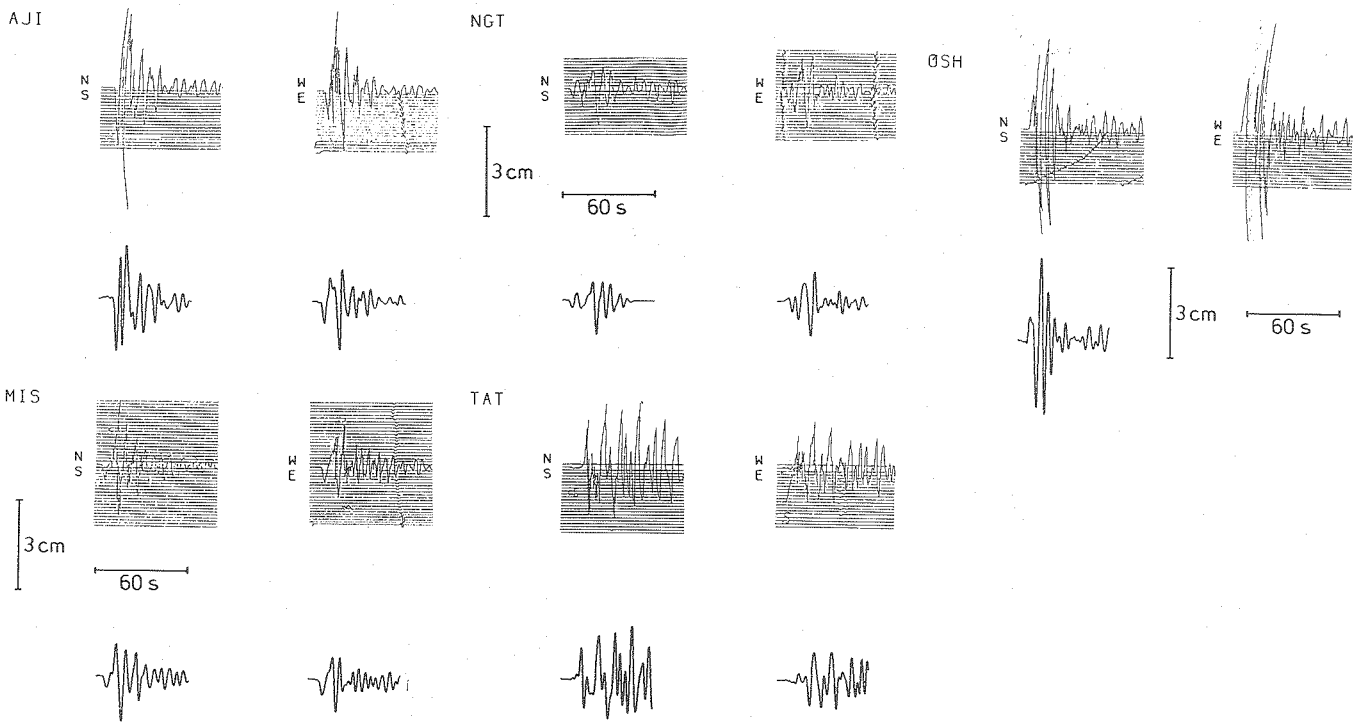

Fig. 2 Strong-motion seismograms used in the present analysis. The upper trace of each pair is the raw record; the lower trace is obtained by processing the upper trace in the manner mentioned in text.

propagates from the hypocenter at a given rupture velocity. The slip angle and the dislocation time history are assumed to be uniform throughout the fault plane.

A synthetic seismogram at a station can be calculated by summing up contributions of all subfaults,

$$\boldsymbol{u}(t)=\sum_{j=1}^{M} m_j \boldsymbol{s}_j(t) \tag{1}$$

where $\boldsymbol{u}(t)$ is the displacement at the station, M the total number of subfaults, m_j the seismic moment of the j-th subfault, and $\boldsymbol{s}_j(t)$ the displacement on the station due to a unit moment on the j-th subfault. The calculation of $\boldsymbol{s}_j(t)$ requires that of a large number of Green functions. These are computed by using the discrete wavenumber/finite element (DWFE) method (Olson et al., 1984), which considers all contributions from body waves, surface waves, leaky modes, and near-field terms, and can take care of gradients as well as discontinuities in the velocity and density structure. This method has a disadvantage that the effects of anelasticity are not easily incorporated, since it is a time domain method. In the present study they are not included. However, the speed of DWFE method in waveform computation may compensate for this drawback, because it is required to do the calculation for many source-receiver combinations in an inversion study of finite source.

3.2 Inversion method

In the present study we apply a least squares waveform inversion technique to retrieve the spatial distribution of the seismic moment release on the fault plane. In order to evaluate the disagreement between the observed and synthetic seismograms, we make use of the following error function originally proposed by Mellman et al. (1975),

$$e(f, g)=1-\phi(\boldsymbol{m}) \tag{2}$$

where $\phi(\boldsymbol{m})$ is a cross correlation between the two functions f and g, and $\boldsymbol{m}$ is the model parameter vector. $\phi(\boldsymbol{m})$ is defined as

$$\phi(\boldsymbol{m})=\max_{\tau} \frac{\int f(t)g(t+\tau)dt}{\left[\int f^2(t)dt \cdot \int g^2(t+\tau)dt\right]^{1/2}} \qquad |\tau| \leq \tau_l \tag{3}$$

where τ is the lag time and τ_l is an upper limit of τ. The error is zero when the function g is proportional to f. We prefer the cross correlation method

with a lag time, since it is very difficult to adjust the timing to match the observed seismograms and the synthetics. This is due to the following fact: only one of horizontal components at each station has time marks, and the other does not. Thus, it is impossible to correlate the time of one component with the time of the other component. Furthermore, uncertainties in crustal velocity and density models assumed in computing the synthetic seismograms cause errors in wave amplitude. The effects of the amplitude error upon inversion results may be minimized by use of the cross correlation method.

The inversion scheme consists of minimizing a weighted sum of the squares of the error functions for all traces, i.e.,

$$\varepsilon = \sum_{i=1}^{N} w_i e_i^2 \tag{4}$$

where N is the number of the traces, and w_i is the weight for the i-th trace. The weight w_i is defined by

$$w_i = \begin{cases} 1.0 \cdot q_i & \text{if : } R_i \leq R_0 \\ \left(\dfrac{R_0}{R_i}\right)^2 \cdot q_i & \text{if : } R_i > R_0 \end{cases} \tag{5}$$

where R_i is the epicentral distance of the i-th trace, and R_0 is a reference distance. The factor q_i is the weight representing the quality of each record. Its value is 1.0 except for the NS-component of AJI which has a little offscale part. A value of 0.5 is selected for the NS-component of AJI. We choose 30 km as R_0 since maximum epicentral distance is approximately 60 km. There are two reasons why we adopt the above expression for the weight. One is that wave amplitudes are approximately proportional to the inverse of epicentral distances. The other is that the larger the epicentral distances become, the more the waveforms are affected by uncertainties in velocity and attenuation structure.

Since the error function e_i is not a linear function of the seismic moment m_j, a non-linear least squares algorithm by Biggs's quasi-Newton method (see, Tanabe, 1980) is used. We make use of the NOLLS 1 code which is a member of the program package NUMPAC (Nagoya University Computation Center, 1982).

4. Application

In order to obtain the information about the seimic fault of the 1980 Izu-Hanto-Toho-Oki earthquake, various investigations have been done, for exam-

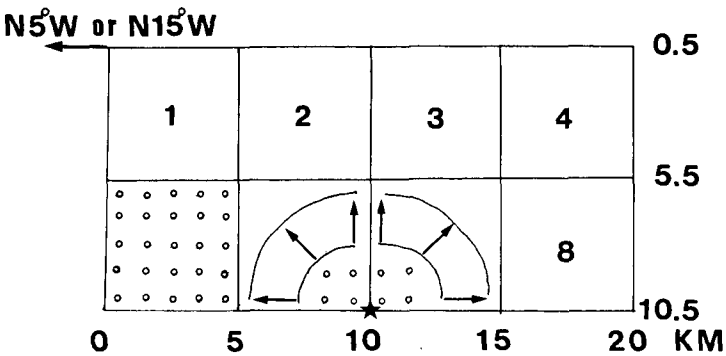

Fig. 3 Fault model used to calculate the synthetic seismograms. 200 point sources are evenly distributed at a spacing of 1 km on the fault plane. Green functions are computed for all the point sources.

Table 2 Instrumental characteristics of JMA strong-motion seismograph

Component	Pendulum Period(sec)	Damping Ratio	Magnification	Length of Arm (cm)	Paper Speed (cm/min)
UD	5	8	1	25	3
NS	6	8	1	30	3
EW	6	8	1	30	3

ple, study of the aftershock distribution (e.g. Matsu'ura, 1983), waveform analysis (e.g. Shimazaki, 1980; Ishida, 1980), and observation of high frequency seismic events by a hydrophone just above the focal region (Mogi and Mochizuki, 1980). Some results from these investigations agree with each other. The basic features are the following:

1. The fault plane is approximately vertical and strikes to nealy NS direction.
2. Its size is approximately 20 km in length and 10 km in width.
3. Source mechanism is left-lateral strike-slip.

In the present study, the fault is assumed to be 20 km in length, extending 10 km to the north and 10 km to the south of the epicenter, and 10 km in width. The fault plane is divided into eight subfaults which are 5 km by 5 km squares. The subfaults are numbered for convenience as shown in Fig. 3. The hypocenter is located at the center of the bottomside of the fault. Rupture mechanism is assumed to be purely left-lateral strike-slip.

Waveforms of near-field strong motions are sensitive to the fault geometry. Since this earthquake occurred below the sea bottom, the precise location and

geometry of the seismic fault cannot be determined. To circumvent this problem, various models with different fault parameters (strike, rupture velocity and rise time) are assumed. Okada (1980) has estimated a strike of N4°W, a rupture velocity of 3.0 km/sec and a rise time of 1.0 sec. Tanaka et al. (1982) has deduced a strike of N5°W from the characteristics of the strong-motion accelerograms. Matsu'ura (1983) has estimated a strike of N20°W from the aftershock distribution. Irikura (1983) has simulated the strong ground motions using a strike of N15°W and a rupture velocity of 3.2 km/sec ; and Sasaki et al. (1983) has used a rupture velocity of 2.5 km/sec to calculate the synthetic seismograms of the main shock. In the present study, strikes of N5°W and N15 °W, rupture velocities of 2.5 km/sec and 3.0 km/sec, and rise times of 1.0, 1.5 and 2.0 sec are used in the inversion. Table 3 lists the combinations of strike, rupture velocity and rise time. Each combinations are named as shown in table 3 (e.g. Model A-1).

Two velocity and density models, as shown in Table 4, are assumed in computing the synthetic seismograms. Both models are identical except at shallow depths (0-4 km). Structure-A has a thin soft sedimentary layer at the top, whereas Structure-B does not. Both models are based on the models produced by Kudo et al. (1978) and Sasaki et al. (1983).

The synthetic seismograms are convolved with the impulse response of the seismograph system, and resampled at an interval of 0.25 sec. These seismograms are filtered with the identical band-pass filter used on the observed

Table 3 List of assumed models

Model Name	Velocity and Density Structure	Strike	Rupture Velocity (km/sec)	Rise Time (sec)
A1	A	N 5°W	3.0	1.0
A2	A	N 15°W	3.0	1.0
B1	B	N 5°W	3.0	1.0
B2	B	N 15°W	3.0	1.0
B3	B	N 5°W	3.0	1.5
B4	B	N 15°W	3.0	1.5
B5	B	N 5°W	3.0	2.0
B6	B	N 15°W	3.0	2.0
B7	B	N 5°W	2.5	1.0
B8	B	N 15°W	2.5	1.0
B9	B	N 5°W	2.5	1.5
B 10	B	N 15°W	2.5	1.5

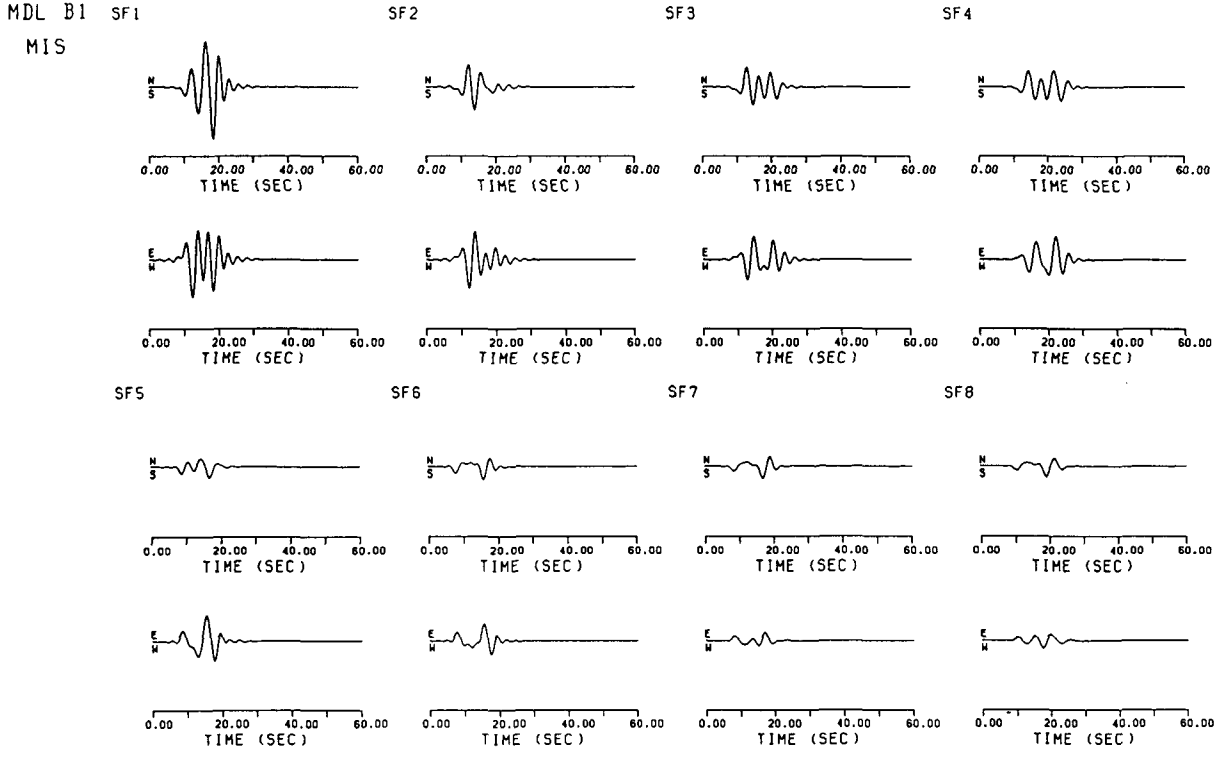

Fig. 4 Synthetic strong-motion displacement due to a unit moment on the j-th subfault, $s_j(t)$, at MIS station for Model-B1. All traces have been convolved with the impulse response of the seismograph system, and filtered by a Chebyshev band-pass filter with a pass-band of 3 to 20 sec.

seismograms. After these processings, the synthetics calculated using Structure-A and B closely resemble each other. Structure-A is used only in Model-A1 and A2, and Structure-B is used in the other models (see Table 3). Figure 4 shows $s_j(t)$ at MIS station for Model-B1, which has been already processed in the above manner. Note that the effects of directivity are very prominent. The function $s_j(t)$ of the other stations is shown in Fig. A1.

The inversion method mentioned above is applied to each model listed in Table 3. We examine whether each solution is physically reasonable according to the following criteria:

$$m_j / \sum_{k=1}^{8} m_k > -0.1 \qquad (j=1, 2, \ldots, 8) \tag{6}$$

$$\varepsilon/N < 0.09 \tag{7}$$

The criterion (6) is based on an idea that significant back slip, i.e. negative moment, should not take place. The criterion (7) is adopted to reject solutions having much error. When the solution doesn't satisfy these criteria, we can conclude that the assmed model is not appropriate. Although the choice of parameter values in these criteria might not be objective, these are nevertheless useful.

5. Results

A starting model of $m_j=1.0$ ($j=1, 2, \ldots, 8$) was taken. Setting $\tau_l=2.5$ sec (see (3)), the first 20 sec of the data traces were inverted for each model listed in Table 4. Four solutions satisfied the criteria of (6) and (7). These are shown in Fig. 5. The absolute values of m_j obtained by the inversions are meaningless, since the error function is insensitive to the absolute amplitudes. (see (2) and (3)). We are concerned only with the ratios of m_j to their total, i.e. $m_j/\sum m_k$. All reasonable solutions are nearly identical. Note that all the reasonable solutions have the strike of N5°W and the rupture velocity of 3.0 km/sec (see Table 3 and Fig. 5). As a representative of the four solutions, the moment distribution on the subfaults for Model-B1 is schematically shown in Fig. 6. The width of the box is proportional to the moment release on each subfault. Subfault-1, 5 and 6 (see Fig. 3, 5 and 6) have little moment, and most of the seismic moment is concentrated on the southern part of the fault plane. This means that there was minimal extension of the rupture front to the north during the mainshock.

The synthetic seismograms for Model-B1 are compared to the data traces

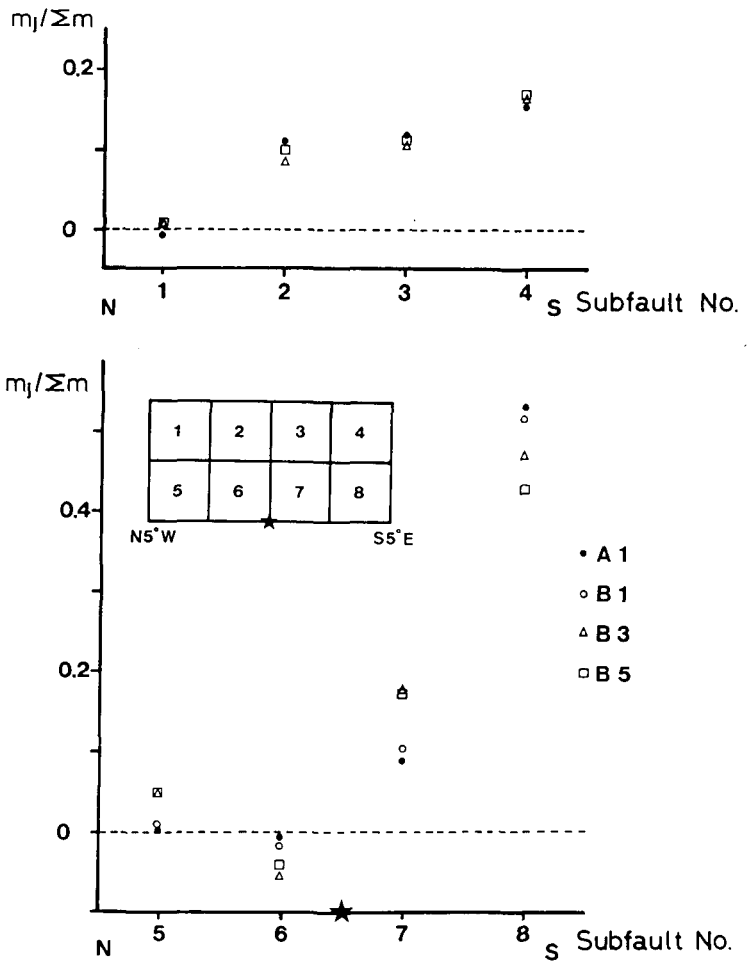

Fig. 5 Reasonable solutions satisfying the criteria of (6) and (7). The diagram inset shows the number assigned to each subfault. The star indicates the hypocenter. The open circles and the solid circles of Subfault-2, 3 and 4 overlap each other.

in Fig. 7. The data and synthetics have been normalised to equal amplitudes to compare the waveforms. In general, the overall features of the data are modeled well, although their details are not reproduced in the synthetics. Our fault models are too simple to explain the details of the data. A more complicated space-time history of the rupture may be required to model the details.

The error ε (see (4)) of the starting model and the final solution are shown in Table 5 for each reasonable model. The final ε decreases with increasing

Table 4 Assumed velocity and density structure

Structure A

Depth (km)	V_p (km/s)	V_s (km/s)	ρ (g/cm^3)
0.0*	2.40	1.00	2.00
0.5*	4.00	2.30	2.50
4.0*	6.40	3.70	2.80
19.0	6.75	3.90	3.00
30.0	7.80	4.50	3.30

Structure B

Depth (km)	V_p (km/s)	V_s (km/s)	ρ (g/cm^3)
0.0*	3.46	2.00	2.40
4.0*	6.40	3.70	2.80
19.0	6.75	3.90	3.00
30.0	7.80	4.50	3.30

Between two successive depths marked by asterisk, velocity and density have linear gradient.

Table 5 List of ε

Model name	Initial ε	Final ε
A1	1.50	0.76
B2	1.49	0.75
B3	1.37	0.64
B5	1.24	0.57

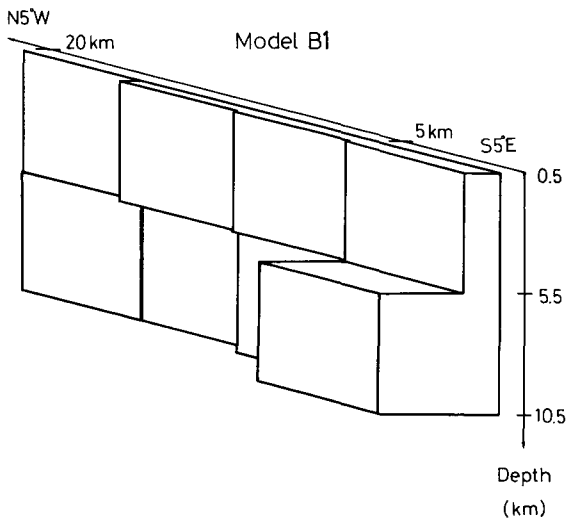

Fig. 6 Diagram of solution for Model-B1. The width of the box on each subfault is proportional to the seismic moment release on it.

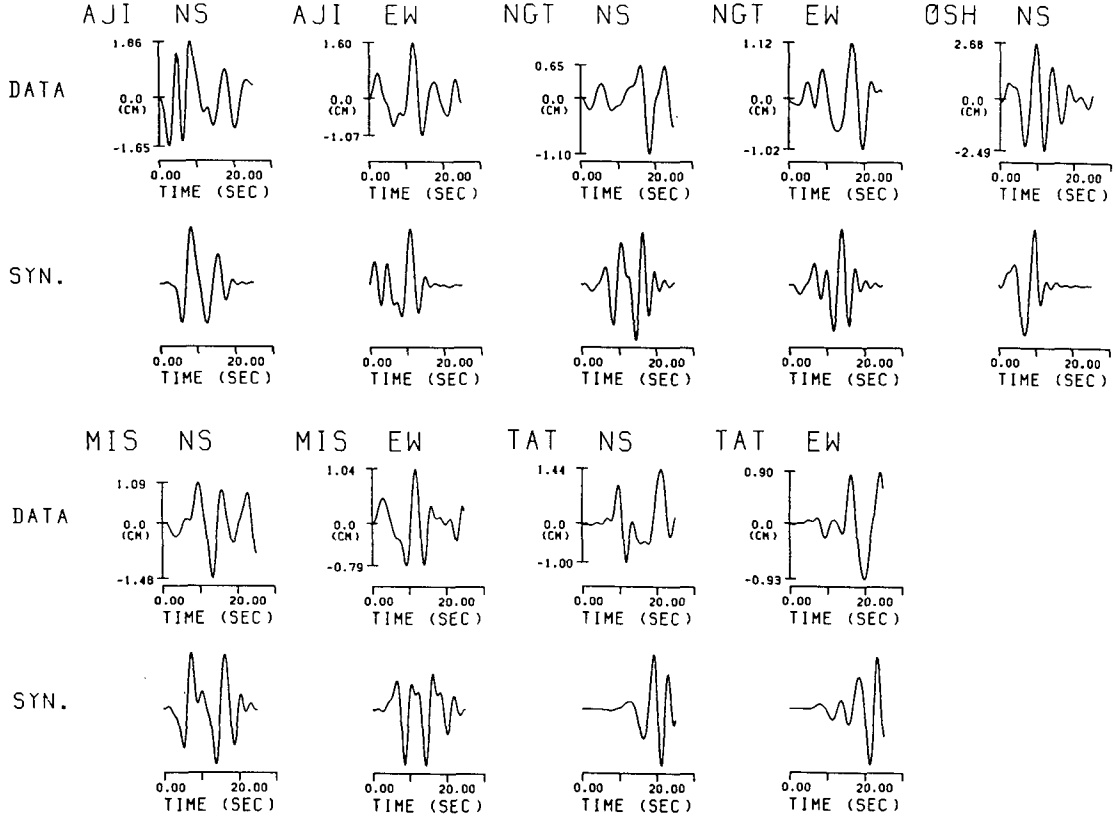

Fig. 7 Comparison of synthetics with the data for Model-B1. The data is the upper trace of each pair of records. Both traces have been normalized to equal amplitudes to compare the waveforms.

rise time. Thus, Model-B5 appears to be the most preferable of the four. However, we should not make a definite conclusion, since this might be mainly due to neglecting the effects of attenuation in computing the synthetic seismograms.

6. Discussion

The reasonable solutions obtained in this study are consistent with Ishida's interpretation (Ishida, 1980). She found that the aftershocks, which were thought to have occurred on the fault plane after the main shock, had waveforms very different from the waveforms of the swarm earthquakes which have occurred during the same period. The epicenters of these aftershocks were distributed within a range of 2 km to the north and 10 km to the south of the mainshock epicenter. Okada (1980) and Sasaki et al. (1983) used the fault-models extending 5 km to the north and 10 km to the south of the epicenter to explain the near-source strong-motion seismograms at Nakaizu station of the National Research Center for Disaster Prevention. Comparing our solutions with the aftershock distribution ($M \geq 2.9$) estimated by Matsu'ura (1983), we noticed that most of the aftershocks having occurred for 10 hours after the mainshock are located within Subfault-2, 3, 4, 7 and 8 (see Fig. 9(b) of Matsu'ura's paper).

The most characteristic feature of the earthquake studied in this paper is that a very active earthquake swarm continued in the area very close to its

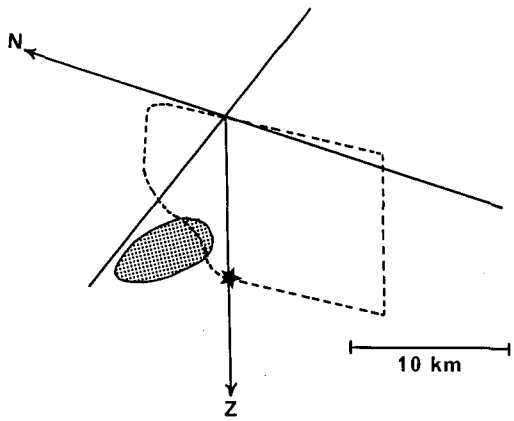

Fig. 8 Spatial diagram of the swarm activity and the fault plane of the mainshock. The shaded region indicates the swarm area. The area enclosed by a broken line is presumed to have been ruptured during the mainshock.

hypocenter just before and after its occurrence. According to Karakama et al. (1980) and Matsu'ura (1983), the swarm activity started with a microearthquake on June 22, 1980 and rapidly developed with repeated burst-type activity of rather short durations. The epicenters of the swarm earthquakes concentrated in a small region, several kilometers in diameter. During this activity, the mainshock took place at 16 : 20 (JST) on June 29, and its hypocenter was located about 3 km south of the concentrated activity. Its aftershocks occurred astride the swarm area. About 10 hours after the mainshock, the burst-type activity before the mainshock was renewed in the same area and repeated intermittently until July 27. Matsu'ura (1983) concluded that the swarm activity before and after the mainshock cannot be regarded as foreshock and aftershock sequences, respectively, and suggested that the swarm area did not overlap the aftershock area. Taking these into account, our solutions suggest that the rupture front of the mainshock could not go across the swarm area. Figure 8 shows a spatial diagram of the swarm activity and the fault plane of the main shock. The area enclosed by a broken line indicates the fault plane, which is presumed to have been ruptured during the main shock from our solutions.

Appendix

The Appendix consists of Figures Al(a) to (d).

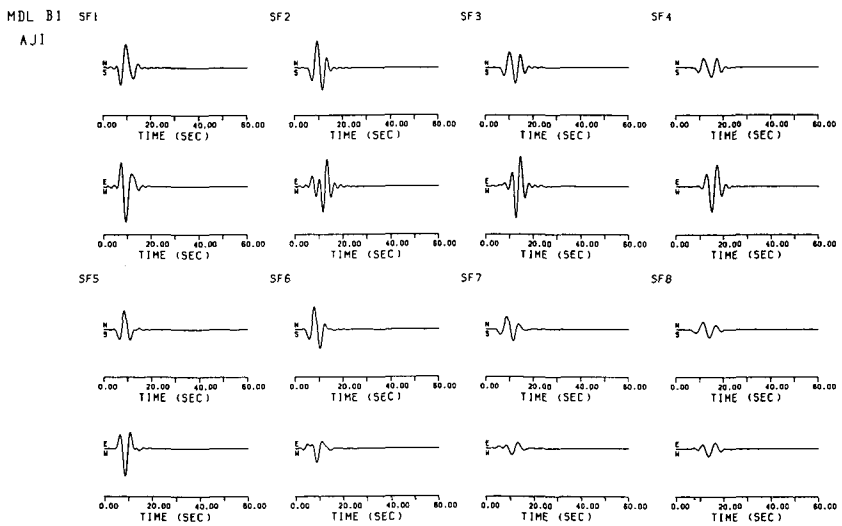

(a)

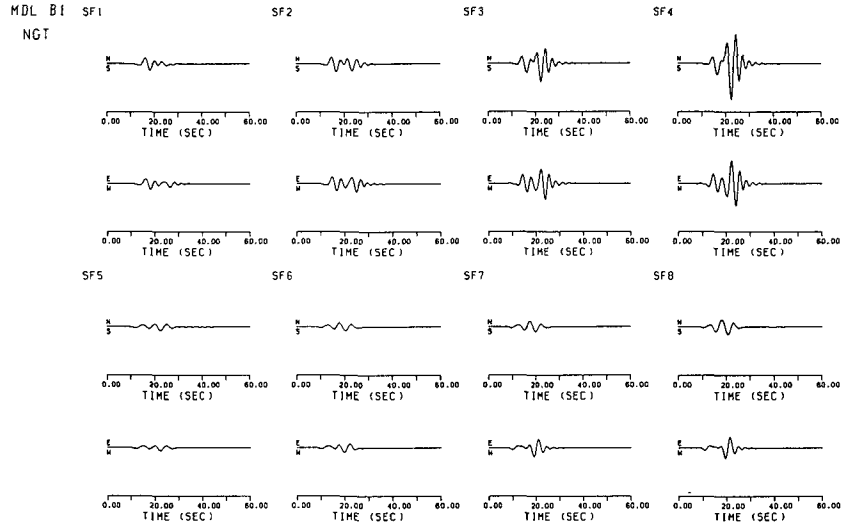
MDL B1
NGT
SF1
SF2
SF3
SF4
SF5
SF6
SF7
SF8
N S
E W
0.00 20.00 40.00 60.00
TIME (SEC)

(b)

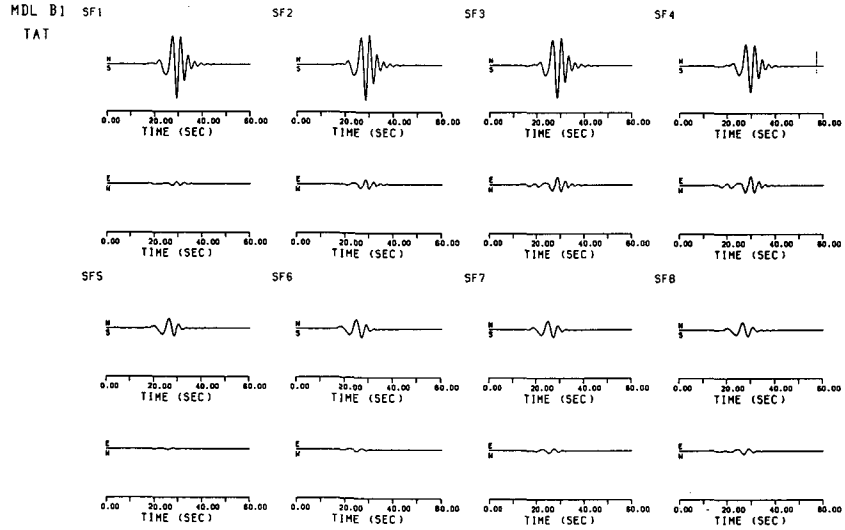
MDL B1
TAT
SF1
SF2
SF3
SF4
SF5
SF6
SF7
SF8
N S
E W
0.00 20.00 40.00 60.00
TIME (SEC)

(c)

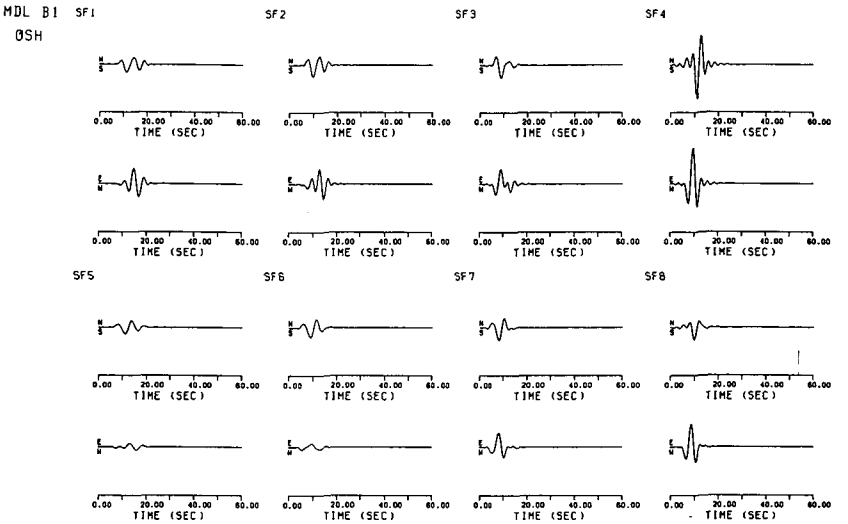

(d)

Fig. A1 Synthetic strong-motion displacement due to a unit moment on the j-th subfault, $s_j(t)$, for Model-B1. See caption of Figure 4 for further explanations. (a) $s_j(t)$ at AJI station. (b) $s_j(t)$ at NGT station. (c) $s_j(t)$ at TAT sation. (d) $s_j(t)$ at OSH station.

Acknowldgements

I would like to thank Prof. I. Yokoyama, Dr. Y. Nishida and Dr. T. Sasatani for their continuous encouragement and giving valuable suggestions. I also thank Dr. I. Nakanishi for critically reading the manuscript and helpful comments. I gratefully thank Dr. M. Takeo of the Meteorological Research Institute for supplying the strong-motion records and giving much useful advice. Finally, I am grateful to Mr. J.P. Catane for his assistance in writing the manuscript in English.

The numerical computations were carried out by HITAC M280H at the Hokkaido University Computing Center.

References

Archuleta, R.J., 1984. A faulting model for the 1979 Imperial Valley earthquake. J. Geophys. Res., **89**, 4559-4585.

Hartzell, S.H. and T.H. Heaton, 1983. Inversion of strong ground motion and teleseismic waveform data for the fault rupture history of the 1979 Imperial Valley, California, earthquake. Bull. Seism. Soc. Am., **73**, 1553-1583.

Hartzell, S.H. and D.V. Helmberger, 1982. Strong-motion modeling of the Imperial Valley

earthquake of 1979. Bull. Seism. Soc. Am., **72**, 571-596.
Irikura, K., 1983. Semi-empirical estimation of strong ground motions during large earthquakes. Bull. Disas. Prev. Res. Inst., Kyoto Univ., **33**, Part 2, 63-104.
Ishida, M., 1980. The swarm activities off the Kawanazaki Point and off the east coast of the Izu Peninsula, and the 1980 Izu-Hanto-Toho-Oki earthquake. Abstract, Fall Meeting Seismol. Soc. Japan, 5 (in Japanese).
Karakama, I., I. Ogino, K. Tsumura, K. Kanjo, M. Takahashi and R. Segawa, 1980. The earthquake swarm east off the Izu Peninsula of 1980. Bull. Earthq. Res. Inst., Univ. Tokyo, **55**, 913-948 (in Japanese with English summary).
Kudo, K., S. Zama, M. Yanagisawa and E. Shima, 1978. On the shear wave underground structure of Izu Peninsula. Bull. Earthq. Res. Inst., Univ. Tokyo, **53**, 779-792 (in Japaese with English summary).
Matsu'ura, S.R., Detailed study of the earthquake sequence in 1980 off the east coast of the Izu Peninsula, Japan. J. Phys. Earth, **31**, 65-101.
Mellman, G.R., L.J. Burdick and D.V. Helmberger, 1975. Determination of source parameters from body wave seismograms. Earthquake Notes, **40**, 44.
Mogi, K. and H. Mochizuki, 1980. Observation of high frequency seismic waves by a hydrophone just above the focal region of the 1980 Izu-Hanto-Toho-Oki earthquake and a precise estimate of location of the submarine earthquake fault. Bull. Earthq. Res. Inst., Univ. Tokyo, **55**, 1017-1041 (in Japanese with English summary).
Nagoya University Computation Center, 1982. User's guide of library programs (volume of numerical computation), Nagoya University Computation Center, Nagoya (in Japanese).
Okada, Y., 1980. Faulting process of the earthquake off the east coast of Izu Peninsula of June 29, 1986. Abstract, Fall Meeting Seismol. Soc. Japan, 9 (in Japanese)
Olson, A.H. and R.J. Apsel, 1982. Finite faults and inverse theory with applications to the 1979 Imperial Valley earthquake. Bull. Seism. Soc. Am., **72**, 1969-2001.
Olson, A.H., J.A. Orcutt and G.A. Frazier, 1984. The discrete wavenumber/finite element method for synthetic seismograms. Geophys. J.R. astr. Soc., **77**, 421-460.
Saito, M., 1978. An automatic design algorithm for band selective recursive digital filters. Butsuri-Tanko (Geophysical Exploration), **31**, 112-135 (in Japanese with English synopsis).
Sasaki, S., Y. Sawada, H. Yajima, Y. Esashi and A. Sakurai, 1983. Calculation of seismic waves for a dislocation source model in a multi-layered medium. Civil Engineering Laboratory Rep., No. 380021, Central Research Institute of Electric Power Industry (in Japanese with English synopsis).
Shimazaki, K., 1980. Fault parameters of the 1980 Izu-Hanto-Toho-Oki earthquake. Abstract, Fall Meeting Seismol. Soc. Japan, 8 (in Japanese).
Tanabe, K., 1980. Algorithms of non-linear least squares method. Oyo-Tokei-Gaku, **9**, 119-140 (in Japanese).
Tanaka, T., S. Yoshizawa, M. Sakaue and Y. Osawa, 1982. Estimation of acceleration characteristics of strong ground motion by synthesis of accelerogram obtained during a small earthquake. Bull. Earthq. Res. Inst., Univ. Tokyo, **57**, 561-579 (in Japanese with English summary).
Yamada, Y., S. Noda and M. Tomimoto, 1985. Characteristics of relatively long-period (5 to 15 sec) ground motions using JMA's seismograph records during the 1983 Nihonkai-Chubu earthquake. Disas. Prev. Res. Inst. Ann., Kyoto Univ., **28B-2**, 33-60 (in Japanese with English synopsis).
Yamanaka, H., K. Seno, T. Sakuma and S. Midorikawa, 1985. Examination of accuracy of JMA's strong mosion seismograph records. Abstract, Fall Meeting Seismol. Soc. Japan, 153 (in Japanese).